Chapter 5 | *Global structure parameters of edge-on disk galaxies*

Abstract. A statistical study of global galaxy parameters can help to improve our understanding of galaxy formation processes. In this Chapter we present the analysis of global galaxy parameters based on optical and near-infrared observations of a large sample of edge-on disk galaxies.
We found a correlation between the ratio of the radial to vertical scale parameter and galaxy type: galaxies become systematically thinner when going from S0's to Sc's, whereas the distribution seems to level off for later types.
The observed scale length ratios (and thus the radial colour gradients) largely represent the galaxies' dust content. On average the colour gradients indicated by scale length ratios increase from type Sa to at least type Sc. For galaxy types later than Sc, the average colour gradient seems to decrease again.
The distribution of K-band (edge-on) disk central surface brightnesses is rather flat, although with a large scatter. However, the latest-type sample galaxies ($T > 6$) show an indication that their average disk central surface brightnesses may be fainter than those of the earlier types. This effect is probably not the result of dust extinction.

1 A statistical analysis

A study of the statistical properties of highly-inclined, or "edge-on" galaxies benefits greatly from the special orientation with respect to the line of sight of such galaxies. Observations of edge-on galaxies provide us with direct measurements of the luminosity and colour distributions both perpendicular to the galaxy planes and along the galaxies' major axes at various heights above the plane. Indirectly, these luminosity distributions can be related to the galaxies' density distributions and thus their global structure. Moreover, in-depth knowledge of the dust distribution, and hence the optical depth of galaxies, is important for our understanding of galaxy evolution.

1.1 The flattening of exponential disks

A major advantage of studying highly-inclined galaxies is that one can determine their radial and vertical scale parameters directly and independently, since the dependence of these parameters on inclination is smallest for the highest inclinations (e.g., van der Kruit & Searle, 1981a; de Grijs et al., 1997 [Chapter 8]). These scale parameters provide us with information about the intrinsic shape of galaxy disks, i.e., their flattening, in a more direct way than the canonical axis ratios. Moreover, since the vertical scale height, $z_0 = 2h_z$, is to first order independent of radius (e.g., van der Kruit & Searle, 1981a,b, 1982a; Kylafis & Bahcall, 1987; Shaw & Gilmore, 1990; Barnaby & Thronson, Jr., 1992; but see de Grijs & Peletier, 1997 [Chapter 7]), the radial to vertical scale parameter ratio, h_R/z_0, can often be determined more accurately than the major to minor axis ratio.

By studying the scale parameter ratio statistically, we may be able to put constraints on the disk formation processes as well as on the stability of galaxy disks (e.g., Bottema, 1993). When considering the physical processes that determine the scale parameters one does not immediately expect a strong correlation between scale length and scale height. The scale height is likely determined by the internal, secular evolution of the stellar velocity dispersion (e.g., van der Kruit & Searle, 1981a; Carlberg, 1987; see also de Grijs et al., 1997 [Chapter 8]), whereas the scale length is basically the result of the composition of the protogalaxy (Fall, 1983; van der Kruit, 1987).

However, one might expect that in a larger disk, with a greater rotation velocity, the heating of the disk stars may be more violent, thus resulting in a larger scale height. Therefore, one may expect a correlation between the rotation velocity (which can be related directly to the scale length) of a galaxy disk and the scale height, although the precise dependence is yet unknown (see, e.g., Bottema, 1993).

Thus, statistics on the ratio of scale length to scale height can be expected to give information on the importance of the formation processes in disk galaxies with different properties.

Moreover, once the h_R/z_0 ratio is known, one may be able to determine the (theoretical) maximum rotation of a disk from measurements of the vertical disk dispersion (Bottema, 1993). Therefore, a statistical treatment of the scale parameter ratio may put general constraints on both the kinematical properties and the global stability of galaxy disks.

Bottema (1993) predicts that a constant value for the h_R/z_0 ratio leads to a more or less constant mass-to-light ratio of the old disk, $(M/L)_B$, under the assumptions that we are dealing with exponential, locally isothermal disks with a constant ratio of vertical to radial velocity dispersion. On the other hand, if we assume a linear relationship between the old-disk absolute luminosity and the vertical velocity dispersion, Bottema (1993) shows that (for a constant $(M/L)_B$) the h_R/z_0 ratio decreases rapidly from faint galaxies to a constant level for normal and bright galaxies. Thus, in general, the observed velocity dispersions imply that a constant old-disk mass-to-light ratio results in an approximately constant scale parameter ratio, whereas a constant scale parameter also leads to mass-to-light ratio that is, to first order, constant.

In fact, these predictions imply that all galaxy disks are governed by equal mass-to-light ratios in the old stellar populations, assuming that all galaxy disks have approximately the same colour (Bottema, 1993).

However, the assumption of a constant and equal mass-to-light ratio of the old-disk population in disk galaxies is probably not physically realistic, considering the range of colours

observed within and among galaxies (e.g., de Jong, 1996c, and references therein). Therefore, the predicted relationships should be treated with caution and only be used as general guidelines.

1.2 Colour gradients as diagnostics

Broad-band colours are relatively easy to obtain and are therefore the most widely used colour diagnostics to date. They immediately reveal the approximate nature of a galaxy, which is to first order determined by its dominant stellar population and dust content.

Although for the detailed analysis of galaxy luminosity and colour profiles one needs to adopt *a priori* assumptions concerning the evolutionary stellar population synthesis, the initial mass function, the metallicity and the star formation history, as well as about the dust geometry and its characteristics, de Jong (1996c) shows that the colours formed from different broad-band combinations correlate strongly, which indicates that these colours are probably caused by the same physical process. Therefore, broad-band colours can be used as indicators of changes in the gross properties of galaxies (e.g., changes in metallicity and/or dust contamination).

All systematic colour differences induced by stellar population changes and metallicity gradients are generally considerably smaller than the reddening due to dust, however.

1.2.1 Radial Colour gradients in edge-on disk galaxies

In contrast to the large number of studies of radial colour gradients in moderately inclined and face-on spiral galaxies (e.g., de Jong, 1996c, and references therein), the colour behaviour of highly-inclined and edge-on galaxies has not received much attention. In highly-inclined galaxies, the study and interpretation of intrinsic colour gradients is severely hampered by the presence of dust in the galaxy planes, which causes the dust lane to appear as a red feature in vertical colour profiles (e.g., de Grijs et al., 1997 [Chapter 8]; see also Chapter 1 for references).

In individual edge-on galaxies, it is generally found that the colours along the major axes, i.e., the locations of the dust lanes, remain nearly constant (e.g., Sasaki, 1987; Wainscoat et al., 1990; Aoki et al., 1991; Peletier & Balcells, 1997), although in most cases the outermost disk regions tend to be slightly bluer on the major axis (e.g., Sasaki, 1987), which may be explained in terms of an increasingly metal-poor population or a decreased amount of dust at larger galactocentric distances. Generally, as the height above the dust lane and its embedded young disk increases, the radial colour gradients become small or statistically insignificant (e.g., Hamabe et al., 1979, 1980; van der Kruit & Searle, 1982a,b; Jensen & Thuan, 1982; Peletier & Balcells, 1997).

1.2.2 Colour gradients from scale length ratios

Since the dust influence varies as a function of passband, scale length ratios could be used as a diagnostic to estimate colour gradients and the dust content of a given galaxy.

Evans (1994) studied the effects of dust on the stellar scale length as a function of wavelength, under the assumption that the resulting scale length differences are solely due to dust absorption. His models predict that these differences are small, at least for face-on galaxies, on the order of the observational uncertainties, and even smaller for galaxies with a prominent bulge component. According to his models, if the scale height ratio between dust and stars is ~ 0.5 (Peletier & Willner, 1992; Evans, 1994), Evans' (1994) models exclude face-on galaxies with $h_B/h_H \approx 2$. On the other hand, larger ratios can be obtained if a galaxy is inclined with respect to the line of sight.

The measurement of blue to red scale length ratios alone will not unambiguously reveal the dust content of a given galaxy, because any deviation from unity can equally well be explained by an intrinsic colour gradient, especially for face-on galaxies (Byun et al., 1994).

2 Approach

In Chapter 2 we described the selection of our sample of highly-inclined disk galaxies, the observations on which the analysis in this Chapter is based and the way we reduced our observational data (see also Peletier, 1993). In this Chapter we will discuss the global photometric and structure properties that we derived from our sample galaxies.

2.1 Determination of the exponential scale length

Knapen & van der Kruit (1991), among others, have shown that the scale lengths of a particular galaxy, determined by different authors, may vary by $\approx 20\%$. The scale length determinations depend heavily on the radial fitting range, which is due to the fact that in general the radial profiles are not exactly exponential. Moreover, a patchy dust distribution in a particular galaxy can easily lead to varying estimates of the scale length, depending on the way the data is reduced (e.g., Giovanelli et al., 1994).

Since we wish to compare scale lengths determined in different passbands within and among galaxies, we need to choose the radial regions over which the disk exponential scale lengths are fitted in a consistent way.

The method that is generally used to determine the scale lengths of disk galaxies is by applying a bulge-disk decomposition algorithm to the azimuthally (elliptically) averaged radial luminosity profiles. However, when dealing with highly-inclined or edge-on galaxies, the results from this technique start to be affected by the vertical as well as the radial luminosity components, which are characterised by significantly different scale parameters. Since the vertical scale height in a typical disk galaxy is generally an order of magnitude smaller than the radial scale length (see Sect. 3.1), the scale lengths derived from elliptically averaged luminosity profiles will be smaller than the true scale lengths.

Also, due to line-of-sight integration, the projection of a radially exponential disk will be a function of the form

$$L(R) = L_0(R/h_R)K_1(R/h_R) \qquad (1)$$

(van der Kruit & Searle, 1981a), where L_0 is the central surface luminosity, R the galactocentric distance, h_R the radial scale length, and K_1 the modified Bessel function of the first kind, which simplifies to

$$(R/h_R)K_1(R/h_R) \;=\; 1 + \frac{R^2}{2h_R^2}\ln(R/2h_R), \quad (R/h_R \ll 1); \qquad (2)$$

$$(R/h_R)K_1(R/h_R) \;=\; \left(\frac{\pi R}{2h_R}\right)^{1/2}\exp(-R/h_R), \quad (R/h_R \gg 1). \qquad (3)$$

in the limits. This means that the projected radial luminosity profile will be flattened towards the galaxy centre. Therefore, unless the projected scale lengths are obtained from the outer parts of the disks only, where $R/h_R \gg 1$, the resulting scale lengths will be estimated too large.

If a strong dust lane is present, the ellipse fitting is severely hampered by extinction effects that are hard to deal with numerically. It is generally assumed that the dust in a galaxy is, just like the stars, distributed in a disk with an exponentially decreasing density as a function of radius, although with a smaller scale height than that of the stellar component (e.g., Disney et al., 1989, among others). Physically, this means that extinction plays a more prominent role near the galaxy centre than in the outer parts, thus resulting in an observed stellar scale length that is larger than the intrinsic scale length.

Although these effects counteract each other, the net result for a given galaxy depends on both the scale parameter ratio and the amount of dust, which both correlate (although weakly) with galaxy type (see, e.g., Sect. 3.1 and de Grijs et al., 1997 [Chapter 8]). However, since the effects are not yet physically well understood, one should try to avoid using the scale lengths obtained from elliptically averaged luminosity profiles.

Alternatively, one can determine the scale length from luminosity profiles extracted at some distance from the galaxy planes and parallel to the galaxies' major axes. The main advantage of such a method is that these profiles are less affected by dust than the elliptically averaged profiles. Moreover, if we assume that the disk thickness is constant to first order, as was argued in Sect. 1.1 (see also de Grijs & van der Kruit, 1996 [Chapter 4]; de Grijs & Peletier, 1997 [Chapter 7]), the intrinsic scale length obtained from the old-disk population at some distance from the plane will be essentially the same as the one at lower z distances. In the plane the situation becomes more complex due to the presence of a young stellar population. However, the young population is generally confined to the region very close to the plane, and likely has a scale height of only $\sim$ 100pc (e.g., Hamabe & Wakamatsu, 1989).

2.2 Determination of the exponential scale height

In the analysis of the vertical light distribution we distinguished between the different sides of the galaxy planes, to avoid possible dust contamination in the case of not perfectly edge-on orientations. In de Grijs & van der Kruit (1996, Chapter 4) the basic reduction process has been described in detail.

In de Grijs et al. (1997, Chapter 8) we show that the vertical profiles are more peaked than expected for an isothermal distribution, and only marginally less peaked than exponential. The analysis shows that we can safely approximate the profile's shape with an exponential distribution at z heights greater than 1.5 scale heights. We fitted the vertical profiles out to 4 scale heights, thereby taking into account the possible presence of underlying thick disk components. Comparison for 24 galaxies with the I–K colour images in de Grijs et al. (1997, Chapter 8) shows that in this vertical region the contamination of the stellar light by dust extinction can also be considered to be negligible.

Furthermore, in this vertical region the results obtained from the B and the I-band data do not differ significantly (de Grijs & Peletier, 1997 [Chapter 7]). Thus, in this region both the red and the blue light is dominated by the old-disk population, and the vertical luminosity profiles are not affected by, e.g., dust or the contribution of a young stellar population.

3 Results

In Table 1 we present the B, I, and K-band scale lengths of our sample galaxies determined from luminosity profiles extracted at positions parallel to the major axes. To obtain these scale lengths, we applied a least-squares minimization algorithm to the luminosity profiles between 1 and 4 K-band radial scale lengths, unless indicated otherwise. The errors we quote are realistic rather than statistical in the sense that they represent the possible deviations from the mean if the radial fitting range is varied.

To obtain luminosity profiles representative of the light distributions parallel to the galaxies' major axes, we decided to extract them at those z distances, on the least dusty side of the planes, where the effects of dust extinction are greatly reduced. In choosing these distances we were limited by the signal-to-noise ratio in the K band. The best choice for the z distance to extract the profiles from turned out to be between 1.0 and 1.5 vertical scale heights. Although the influence of the central dust lane is greatly reduced at these distances from the planes, it is not completely negligible, however.

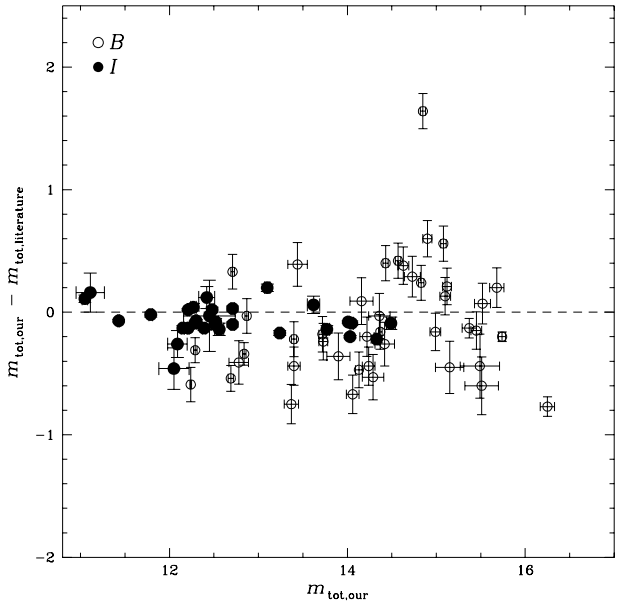

Fig. 2. Comparison of our B- and I-band magnitudes to those published in the RC3 (B band) and by Mathewson et al. (1992, I band). The dashed line indicates the locus of equality.

We used heliocentric velocities obtained by Mathewson et al. (1992) for the majority of our sample galaxies to base the calculation of our distance-dependent parameters on. The effects of the large-scale Hubble expansion were corrected for using Richter et al.'s (1987) formalism, which supposedly yields highly reliable values (Schmidt & Boller, 1992; see also Chapter 6).

Table 1. Scale parameters of the sample galaxies

Columns: (1) Galaxy name (ESO-LV); (2) and (3) I-band exponential scale height (the errors are of order 0.″03); (4)–(7) B-band exponential scale length and measurement error; (8)–(11) I-band exponential scale length and measurement error; (12)–(15) K'-band exponential scale length and measurement error; (16); Maximum rotational velocity (Mathewson et al., 1992).
All values were obtained using a radial fitting range between 1 and 4 K-band (or I-band if no K-band data was available) scale lengths, $h_{R,K}$.

Galaxy			B band				I band				K band				
name	$h_{z,I}$		$h_{R,B}$	$\pm$	$h_{R,B}$	$\pm$	$h_{R,I}$	$\pm$	$h_{R,I}$	$\pm$	$h_{R,K}$	$\pm$	$h_{R,K}$	$\pm$	$v_{\rm rot,max}$
(ESO)	(″)	(h^{-1} kpc)	(″)		(h^{-1} kpc)		(″)		(h^{-1} kpc)		(″)		(h^{-1} kpc)		(km s^{-1})
(1)	(2)	(3)	(4)	(5)	(6)	(7)	(8)	(9)	(10)	(11)	(12)	(13)	(14)	(15)	(16)
026-G06	3.40	0.38	31.84	4.70	3.58	0.53	26.21	2.94	2.95	0.33	18.69	2.05	2.10	0.23	100
033-G22[1]	2.45	0.47	40.52	3.42	7.72	0.65	22.12	1.23	4.21	0.23	—	—	—	—	113
041-G09	4.42	0.76	42.62	2.74	7.36	0.47	35.16	1.80	6.07	0.31	37.75	2.10	6.52	0.36	182
074-G15[2]	10.84	0.22	231.68	48.82	4.83	1.02	173.23	27.92	3.61	0.58	—	—	—	—	—
138-G14[2]	7.21	1.16	107.67	22.44	17.33	3.61	60.91	6.91	9.80	1.11	42.12	14.36	6.78	2.31	106
141-G27	4.16	0.29	49.87	5.00	3.51	0.35	37.42	3.01	2.63	0.21	25.98	4.87	1.83	0.34	87
142-G24	5.78	0.57	45.44	1.26	4.47	0.12	35.49	0.79	3.49	0.08	29.75	1.15	2.93	0.11	121
157-G18	5.01	0.33	49.22	2.29	3.20	0.15	38.53	0.99	2.50	0.06	36.19	1.78	2.35	0.12	91
201-G22	3.01	0.65	31.08	0.81	6.67	0.17	21.98	0.42	4.72	0.09	19.62	0.82	4.21	0.18	165
202-G35	3.44	0.26	24.40	2.44	1.81	0.18	21.22	1.08	1.57	0.08	—	—	—	—	116
235-G53	6.07	1.49	29.92	8.12	7.32	1.99	23.45	3.64	5.74	0.89	—	—	—	—	—
240-G11	3.77	0.62	67.87	4.24	11.15	0.70	41.34	1.57	6.79	0.26	—	—	—	—	241
263-G15	3.49	0.37	60.35	6.40	6.47	0.69	36.09	2.03	3.87	0.22	32.24	2.15	3.45	0.23	—
263-G18	2.95	0.56	32.85	2.56	6.21	0.48	24.27	1.59	4.59	0.30	—	—	—	—	—
269-G15	3.30	0.54	33.30	1.16	5.42	0.19	24.96	0.82	4.07	0.13	—	—	—	—	176
286-G18	3.65	1.67	20.19	0.76	9.21	0.35	17.55	0.46	8.01	0.21	15.57	0.69	7.10	0.31	323
288-G25[1]	3.46	0.41	19.18	0.37	2.28	0.04	17.70	0.34	2.10	0.04	—	—	—	—	—
311-G12	6.05	0.28	28.53	0.38	1.18	0.02	28.74	0.46	1.18	0.02	29.26	0.85	1.21	0.04	—
315-G20	4.01	0.88	22.67	2.48	4.99	0.55	19.36	1.30	4.26	0.29	18.16	5.52	4.00	1.21	—
321-G10	2.73	0.38	14.81	0.38	2.03	0.05	13.80	0.27	1.89	0.04	—	—	—	—	145
322-G73	5.01	1.22	16.65	0.98	2.87	0.17	11.59	0.70	1.99	0.12	—	—	—	—	—
322-G87	2.68	0.35	17.01	0.52	2.21	0.07	14.69	0.37	1.91	0.05	—	—	—	—	149
340-G08	2.23	0.32	18.06	0.48	2.63	0.07	13.40	0.23	1.95	0.03	—	—	—	—	99
340-G09	4.24	0.50	19.08	0.80	2.26	0.09	16.87	0.61	2.00	0.07	12.28	0.77	1.45	0.09	96
358-G26	6.19	0.46	12.84	0.20	0.95	0.01	13.10	0.20	0.97	0.01	—	—	—	—	—
358-G29[1]	6.95	0.56	12.64	0.30	1.02	0.02	12.88	0.32	1.04	0.03	14.73	0.90	1.19	0.07	160
377-G07	3.59	—	41.44	7.12	—	—	33.85	4.65	—	—	—	—	—	—	—
383-G05	8.85	1.46	36.78	3.17	6.06	0.52	28.18	1.39	4.65	0.23	21.36	1.09	3.52	0.18	—
416-G25[1]	3.47	0.96	12.94	0.66	3.59	0.18	11.28	0.49	3.13	0.13	8.82	0.21	2.45	0.06	209
435-G14	2.90	0.52	25.71	1.56	4.62	0.28	16.66	0.55	3.00	0.10	15.88	0.82	2.86	0.15	162
435-G25	4.98	0.57	88.08	4.63	10.16	0.53	51.25	2.17	5.91	0.25	44.09	1.76	5.09	0.20	201
435-G50	2.32	0.27	18.22	0.74	2.14	0.09	14.40	0.46	1.69	0.05	—	—	—	—	79
437-G62	5.31	0.66	30.42	1.67	3.77	0.21	25.77	0.84	3.20	0.10	21.52	0.64	2.67	0.08	—
444-G21	2.33	0.43	14.60	2.47	2.72	0.46	15.94	1.82	2.97	0.34	—	—	—	—	109
446-G18	2.27	0.55	22.38	0.64	5.38	0.15	16.60	0.36	3.99	0.09	14.27	0.43	3.43	0.10	190
446-G44	2.56	0.40	52.00	5.05	8.17	0.79	27.88	1.08	4.38	0.17	18.91	0.45	2.97	0.07	151
460-G31	3.74	0.97	38.36	4.72	9.95	1.22	26.26	1.92	6.81	0.50	19.01	1.35	4.93	0.35	225
487-G02[2]	4.71	0.48	24.09	0.42	2.44	0.04	21.66	0.39	2.19	0.04	22.92	0.57	2.32	0.06	154
500-G24	5.09	0.53	17.00	0.21	1.76	0.02	17.35	0.31	1.80	0.03	19.73	0.79	2.05	0.08	—
505-G03	3.14	0.20	55.78	8.44	3.52	0.53	37.46	3.79	2.36	0.24	—	—	—	—	89
506-G02	3.12	0.75	31.64	5.15	7.59	1.24	22.44	2.98	5.39	0.71	—	—	—	—	208
509-G19	3.64	1.86	23.03	1.88	11.74	0.96	17.39	1.14	8.86	0.58	18.52	2.07	9.44	1.06	—
531-G22	3.13	0.55	25.81	0.84	4.55	0.15	21.27	0.82	3.75	0.14	—	—	—	—	177
555-G36[2]	3.31	—	—	—	—	—	—	—	—	—	—	—	—	—	—
564-G27	3.26	0.46	67.07	5.21	9.43	0.73	37.96	1.08	5.34	0.15	40.59	1.85	5.71	0.26	162
575-G61	3.27	0.31	25.25	1.38	2.39	0.13	18.40	0.36	1.74	0.03	—	—	—	—	65

NOTES:

[1] These galaxies show an additional component, a "lens", with a luminosity profile in between the bulge and the disk component. The fits were applied to the following fitting ranges: ESO033-G22 — 2–4 $h_{R,I}$; ESO288-G25 – 2–6 $h_{R,I}$; ESO358-G29 and ESO416-G25 — 2–6 $h_{R,K}$.

[2] These galaxies are either greatly affected by foreground stars (ESO138-G14, fits between 2 and 4 $h_{R,K}$, and ESO555-G36), have a disk that cannot be approximated well by an exponential luminosity decline (ESO487-G02, fits between 1 and 3 $h_{R,K}$), or show a very irregular radial profile (ESO074-G15, fits between 0 and 2 $h_{R,I}$)

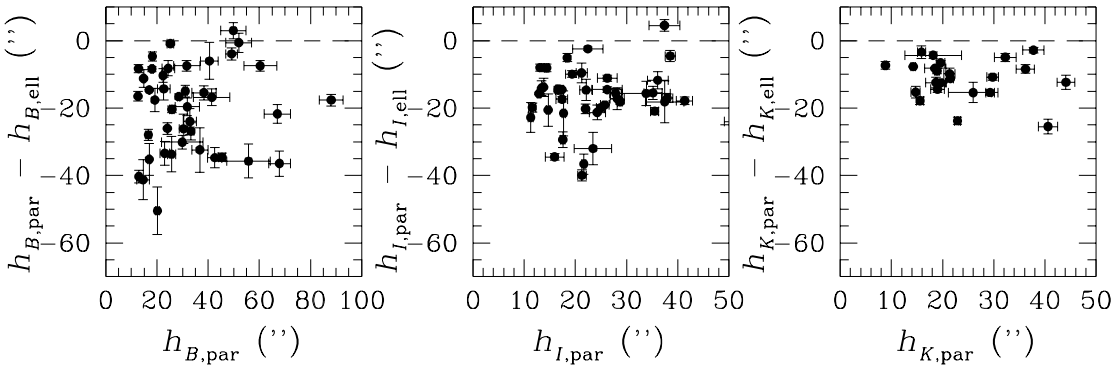

Fig. 1. Comparison between the scale lengths determined using elliptically averaged luminosity profiles ($h_{<\mathrm{band}>,\mathrm{ell}}$) and profiles extracted parallel to the galaxies' major axes ($h_{<\mathrm{band}>,\mathrm{par}}$). The dashed lines indicate the locus of the data points if there were no difference between the two methods.

As already touched upon in Sect. 2.1, since the effects that influence the determination of the scale lengths from elliptically averaged luminosity profiles of edge-on disk galaxies are not well understood, and may even be dependent on galaxy type, they should preferably not be used in an analysis involving global scale parameters. To assess the importance of the effects discussed in Sect. 2.1, in Fig. 1 we compare the scale lengths derived from our sample galaxies using both methods. We notice clear systematic effects in all passbands, in the sense that the scale lengths obtained from the "elliptical" profiles are generally larger than those determined from the "parallel" profiles. The effect is smallest in the near-infrared, indicating that it is probably caused by dust contamination.

Although the ellipse fits should preferably not be used to derive scale parameters from the observed galaxy images, they are useful in providing estimates for the (edge-on) central surface brightnesses of galaxy disks. In Table 2 we tabulate the extrapolated edge-on disk central surface brightnesses.

The calibration of the observations was discussed in Chapter 2. It was shown that our data agree sufficiently well in detail with those published previously. In this Chapter we present, in Table 3, the apparent magnitudes in the *B, I,* and *K* bands of the total galaxies as well as those of the disk components only. The apparent disk magnitudes are based on model disks obtained from ellipse fits to the outer galaxy isophotes.

In Fig. 2 we compare the (total) apparent *B*- and *I*-band magnitudes with literature values; we took the apparent *B*-band magnitudes from de Vaucouleurs et al. (1991, RC3), and the apparent *I*-band magnitudes from the observations by Mathewson et al. (1992). Especially our determinations of the *I*-band apparent magnitudes agree rather well with those determined by Mathewson et al. (1992): the mean deviation between our and Mathewson et al.'s (1992) magnitude determinations is -0.07 ± 0.13 mag (based on a comparison of 30 galaxies); in the *B* band a larger scatter (of 0.45 mag, for 43 galaxies) between our and the RC3 determinations was found, although we do not detect a systematic difference between our apparent *B*-band magnitudes and the RC3 magnitudes (the mean deviation equals -0.09 mag).

In Table 3, we also present the absolute magnitudes in the *I* and *K* bands, M_I and M_K. We did not include the *B*-band absolute magnitudes, as those are too heavily affected by the internal dust extinction to be reliable.

3.1 Scale parameter ratios

Fig. 3 shows the dependence of the scale parameter ratio on galaxy type; we have also plotted the average scale parameter ratios per galaxy type. We notice a correlation between the h_R/z_0 ratio and revised Hubble type, in the sense that galaxies become systematically thinner when going from S0's to Sc's ($T = 5$), whereas the later types (Sd's, $T = 7$) seem to be at least as thin as the Sc's.

Although a correlation between the h_R/z_0 ratio and the rotation velocity was expected, based on the qualitative arguments presented in Sect. 1.1, we do not find any evidence for such a dependence (Fig. 4*b*), nor do we find any evidence for a relationship between the h_R/z_0 ratio and the absolute magnitudes (Fig. 4*c*). In other words, the theoretical prediction that the scale parameter should decrease rapidly from faint galaxies to a constant level for normal and bright galaxies (Bottema, 1993) could not be confirmed observationally. This implies that either the relationship is weak, i.e., smaller than the observational scatter, or the underlying assumptions (of, e.g., a constant $(M/L)_B$, and a linear relationship between the old-disk absolute magnitude and the disk vertical velocity dispersion) either have a large intrinsic scatter themselves or are not valid.

3.2 Radial colour gradients

As we argued in Sect. 1.2.1, one can study radial colour gradients within galaxies by comparing scale lengths determined in different passbands. In Fig. 5 we show the scale length ratios (indicating radial colour gradients) obtained for our sample galaxies.

In Table 4 we present the mean scale length ratios, both for our total sample and for the galaxies of type $T > 2$.

The main conclusion that we draw in de Grijs et al. (1997, Chapter 8), based on the "elliptical" *I* versus *K*-band scale length ratios, still holds firmly, namely that on average the colour gradients indicated by the scale length ratios increase from type Sb ($T = 3$) to at least type Scd ($T = 6$), as is best seen in Figs. 5*a* and *b*. The effect may even be seen in

Table 3. Photometric characteristics of the sample galaxies

Columns: (1) Galaxy name (ESO-LV); (2)–(5), (6)–(9), (10)–(13) Apparent magnitudes of the total galaxy and the disk component only, and the 1σ observational errors, for the B, I and K bands (both determined in Chapter 6), respectively. The systematic errors due to variations in the photometric accuracy are of order 0.07 mag in B, 0.04 mag in I, and 0.08 mag in K; (14)–(16) Galactic extinction in the B band (taken from the RC3), the I and the K bands, respectively; (17)–(18) I and K-band absolute magnitudes, corrected for Galactic extinction (The B-band absolute magnitudes are generally heavily affected by dust extinction and have therefore not been included).

Galaxy	B-band magnitudes				I-band magnitudes				K-band magnitudes				$A_{G,B}$	$A_{G,I}$	$A_{G,K}$	M_I^0	M_K^0
(ESO)	total	±	disk	±	total	±	disk	±	total	±	disk	±	(B, I, K mag)				
(1)	(2)	(3)	(4)	(5)	(6)	(7)	(8)	(9)	(10)	(11)	(12)	(13)	(14)	(15)	(16)	(17)	(18)
026-G06	15.68	0.08	15.80	0.08	13.24	0.02	13.48	0.08	11.50	0.09	11.69	0.10	0.47	0.17	0.04	−18.76	−20.37
033-G22	15.37	0.08	15.51	0.03	14.03	0.01	14.33	0.06	—	—	—	—	0.43	0.16	0.04	−19.10	—
041-G09	13.52	0.01	13.52	0.01	12.21	0.01	12.21	0.03	—	—	—	—	0.62	0.23	0.05	−20.78	—
138-G14	14.85	0.03	15.20	0.05	14.01	0.01	14.37	0.03	—	—	—	—	0.60	0.22	0.05	−18.82	—
141-G27	14.57	0.03	14.57	0.03	12.71	0.02	12.83	0.04	10.57	0.12	10.57	0.12	0.21	0.08	0.02	−18.18	−20.26
142-G24	14.43	0.03	14.43	0.03	12.30	0.01	12.30	0.03	10.56	0.16	10.56	0.16	0.25	0.09	0.02	−19.33	−21.00
157-G18	13.72	0.04	13.72	0.04	12.29	0.02	12.29	0.02	9.79	0.50	9.79	0.50	0.00	0.00	0.00	−18.35	−20.85
201-G22	14.06	0.07	14.06	0.07	13.10	0.03	13.10	0.05	10.34	0.16	10.34	0.16	0.00	0.00	0.00	−20.13	−22.89
202-G35	12.71	0.02	12.71	0.02	11.79	0.02	11.79	0.04	—	—	—	—	0.00	0.00	0.00	−19.13	—
235-G53	14.37	0.02	15.46	0.06	12.45	0.01	13.19	0.04	—	—	—	—	0.09	0.03	0.01	−21.10	—
240-G11	13.44	0.11	13.66	0.11	11.11	0.16	11.50	0.06	—	—	—	—	0.04	0.01	0.00	−21.55	—
263-G15	14.22	0.08	14.22	0.08	11.19	0.01	11.19	0.01	9.09	0.15	9.09	0.15	1.24	0.45	0.11	−20.98	−22.74
263-G18	14.29	0.12	14.33	0.12	11.70	0.02	13.22	0.11	—	—	—	—	0.62	0.23	0.05	−21.49	—
269-G15	14.16	0.13	14.16	0.13	12.15	0.02	12.15	0.04	—	—	—	—	0.47	0.17	0.04	−20.65	—
286-G18	14.90	0.05	14.90	0.05	12.21	0.01	12.21	0.03	10.45	0.38	10.45	0.38	0.07	0.03	0.01	−22.69	−24.43
288-G25	13.73	0.05	13.73	0.05	11.62	0.01	11.62	0.03	—	—	—	—	0.00	0.00	0.00	−20.33	—
311-G12	12.24	0.01	13.32	0.03	10.04	0.01	10.85	0.03	7.35	0.20	8.36	0.61	1.49	0.54	0.13	−20.15	−22.43
315-G20	16.25	0.08	17.56	0.40	12.62	0.01	13.76	0.07	9.19	0.78	11.03	0.98	0.00	0.00	0.00	−20.67	−24.10
321-G10	13.90	0.13	14.84	0.07	12.05	0.17	12.05	0.15	—	—	—	—	0.35	0.13	0.03	−20.34	—
322-G73	13.37	0.08	13.68	0.09	11.84	0.02	12.26	0.02	—	—	—	—	0.52	0.19	0.04	−21.10	—
322-G87	14.24	0.07	14.24	0.07	12.09	0.11	12.09	0.11	—	—	—	—	0.49	0.18	0.04	−20.23	—
340-G08	15.52	0.09	16.22	0.04	13.77	0.03	13.95	0.04	—	—	—	—	0.16	0.06	0.01	−18.68	—
340-G09	15.08	0.03	15.08	0.03	13.62	0.07	13.62	0.07	11.34	0.63	11.34	0.63	0.20	0.07	0.02	−18.39	−20.62
358-G26	12.87	0.02	13.11	0.02	11.68	0.01	12.84	0.04	—	—	—	—	0.00	0.00	0.00	−19.23	—
358-G29	12.29	0.02	13.14	0.04	10.37	0.01	11.08	0.04	8.26	0.29	9.16	0.74	0.00	0.00	0.00	−20.73	−22.84
377-G07	15.49	0.22	15.49	0.22	13.49	0.07	13.49	0.09	—	—	—	—	0.34	0.12	0.03	—	—
383-G05	14.63	0.06	14.87	0.08	11.94	0.02	12.62	0.05	8.95	1.15	9.72	0.24	0.16	0.06	0.01	−20.78	−23.72
416-G25	14.42	0.11	14.65	0.04	12.52	0.03	12.81	0.05	10.35	0.76	11.38	1.12	0.03	0.01	0.00	−21.28	−23.44
435-G14	14.73	0.09	14.73	0.09	12.56	0.05	12.56	0.08	10.12	0.37	10.12	0.37	0.18	0.07	0.02	−20.36	−22.75
435-G25	12.78	0.11	13.23	0.14	11.05	0.03	11.54	0.07	8.42	0.41	8.63	0.52	0.25	0.09	0.02	−20.92	−23.48
435-G50	15.74	0.04	15.74	0.04	14.33	0.03	14.33	0.05	—	—	—	—	0.29	0.11	0.02	−17.70	—
437-G62	12.69	0.03	13.47	0.07	10.72	0.01	11.28	0.03	8.34	0.19	8.65	0.11	0.31	0.11	0.03	−21.43	−23.73
444-G21	15.15	0.16	15.15	0.16	14.05	0.02	14.05	0.03	—	—	—	—	0.25	0.09	0.02	−18.96	—
446-G18	15.12	0.05	15.32	0.06	12.71	0.02	13.21	0.04	10.17	0.42	10.84	0.42	0.22	0.08	0.02	−20.85	−23.33
446-G44	14.83	0.03	14.83	0.03	12.51	0.04	12.51	0.06	10.23	0.66	10.23	0.66	0.29	0.11	0.02	−20.15	−22.34
460-G31	14.99	0.06	15.39	0.09	12.48	0.02	13.28	0.03	10.02	0.56	10.55	0.60	0.71	0.26	0.06	−21.42	−23.68
487-G02	13.40	0.03	13.66	0.04	11.43	0.01	11.49	0.03	8.84	0.39	9.05	0.82	0.04	0.01	0.00	−20.18	−22.76
500-G24	12.84	0.02	13.25	0.03	10.92	0.01	11.31	0.03	—	—	—	—	0.34	0.12	0.03	−20.85	—
505-G03	13.40	0.07	13.40	0.07	12.39	0.02	12.39	0.04	—	—	—	—	0.25	0.09	0.02	−18.27	—
506-G02	14.13	0.04	14.37	0.27	12.45	0.29	13.06	0.11	—	—	—	—	0.46	0.17	0.04	−21.19	—
509-G19	15.10	0.06	15.10	0.06	12.32	0.01	12.32	0.04	9.58	0.44	9.58	0.44	0.21	0.08	0.02	−22.87	−25.55
531-G22	13.96	0.08	13.96	0.08	12.27	0.03	12.27	0.06	—	—	—	—	0.10	0.04	0.01	−20.58	—
555-G36	15.45	0.06	15.45	0.06	14.18	0.03	14.18	0.06	—	—	—	—	0.47	0.17	0.04	—	—
564-G27	14.36	0.12	14.56	0.12	12.42	0.09	13.02	0.11	9.72	0.34	9.72	0.34	0.56	0.20	0.05	−20.09	−22.64
575-G61	15.51	0.19	15.51	0.19	14.49	0.05	14.49	0.08	—	—	—	—	0.25	0.09	0.02	−17.05	—

Table 2. Extrapolated central surface brightnesses
All values were obtained using a radial fitting range between 1 and 4 K-band (or I-band if no K-band data was available) scale lengths, $h_{R,K}$.

Galaxy	$\mu_{0,B}$	±	$\mu_{0,I}$	±	$\mu_{0,K}$	±
(ESO-LV)	(B, I, K mag arcsec^{-2})					
(1)	(2)	(3)	(4)	(5)	(6)	(7)
026-G06	22.16	0.15	20.11	0.14	17.54	0.10
033-G22	22.37	0.41	20.66	0.51	—	—
041-G09	22.28	0.22	19.44	0.10	16.45	0.05
074-G15	21.13	0.18	19.55	0.08	—	—
138-G14	20.70	0.10	19.51	0.07	18.34	0.52
141-G27	21.55	0.06	19.66	0.06	17.11	0.03
142-G24	20.42	0.09	19.12	0.17	17.37	0.12
157-G18	21.25	0.08	19.29	0.07	16.02	0.04
201-G22	19.36	0.67	18.28	0.11	—	—
202-G35	22.81	0.28	22.02	0.87	—	—
235-G53	21.64	0.13	19.16	0.42	—	—
240-G11	21.94	0.17	18.82	0.15	15.77	0.13
263-G15	22.08	0.23	19.49	0.24	—	—
263-G18	21.42	0.17	18.83	0.08	—	—
269-G15	21.54	0.17	19.33	0.11	16.34	0.14
286-G18	20.03	0.18	18.53	0.30	—	—
288-G25	20.14	0.10	18.04	0.04	15.53	0.19
311-G12	23.10	0.21	19.72	0.32	15.98	0.12
315-G20	19.92	0.18	18.51	0.36	—	—
321-G10	21.43	0.32	19.75	0.28	—	—
322-G73	21.44	0.45	18.95	0.45	—	—
322-G87	21.12	0.10	20.18	0.17	—	—
340-G08	20.34	0.43	21.45	0.17	19.19	0.59
340-G09	18.21	0.06	16.16	0.05	—	—
358-G26	19.13	0.19	17.36	0.22	15.66	0.36
358-G29	22.22	0.62	20.95	0.52	—	—
377-G07	22.60	0.13	19.92	0.12	16.24	0.10
383-G05	21.59	0.38	19.47	0.30	16.18	0.65
416-G25	20.65	0.09	18.44	0.08	15.84	0.26
435-G14	21.69	0.22	18.73	0.24	15.49	0.11
435-G25	20.51	0.05	19.73	0.05	—	—
435-G50	20.37	0.33	18.13	0.05	15.20	0.09
437-G62	20.86	0.39	20.57	0.26	—	—
444-G21	20.90	0.09	18.78	0.13	15.40	0.09
446-G18	20.96	0.09	18.74	0.05	15.79	0.03
446-G44	22.49	0.20	19.82	0.09	16.93	0.12
460-G31	20.53	0.06	18.64	0.07	15.83	0.12
487-G02	19.54	0.04	17.84	0.06	15.79	0.06
500-G24	20.58	0.08	19.39	0.18	—	—
505-G03	20.46	0.11	18.39	0.13	—	—
506-G02	21.59	0.09	18.83	0.07	15.61	0.04
509-G19	20.77	0.23	19.54	0.24	—	—
531-G22	21.73	0.11	20.54	0.15	—	—
555-G36	23.26	0.37	19.60	0.30	16.96	0.14
564-G27	21.34	0.11	20.29	0.13	—	—

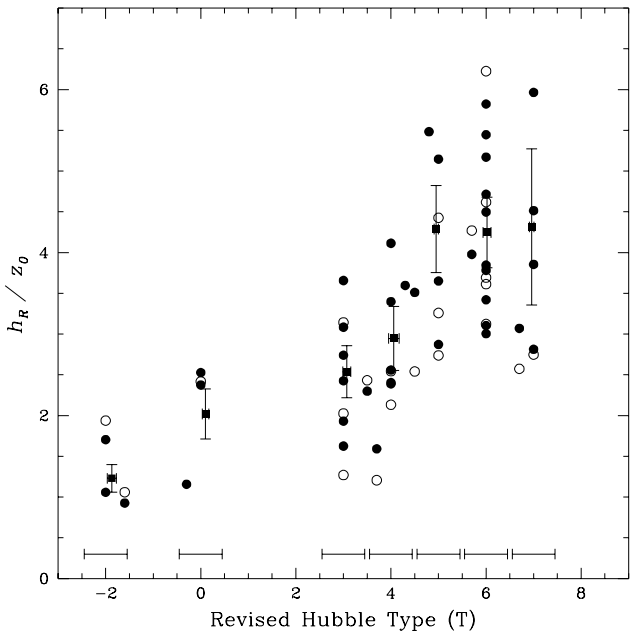

Fig. 3. Dependence of the h_R/z_0 ratio on galaxy type for both I-band data (filled dots) and K-band observations (open circles). The filled squares show the I-band ratios averaged over the type bins indicated by the horizontal bars; the errors indicate the standard deviations of the distribution.

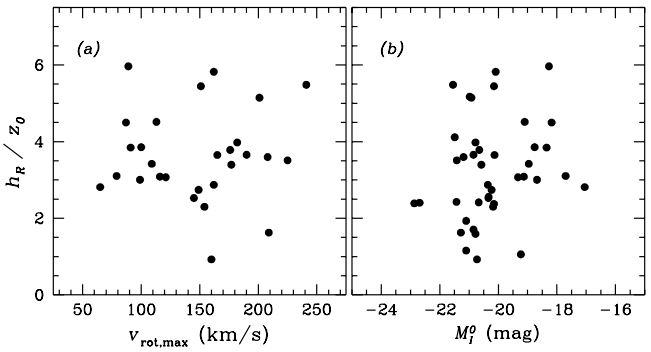

Fig. 4. I-band scale parameters versus *(a)* the maximum rotation velocity, and *(b)* the absolute I-band magnitudes.

Fig. 5*c*. For galaxy types later than Scd, the colour gradients seem to become smaller again, although – due to small-number statistics – we cannot draw any firm conclusions in that range of galaxy types.

For the earliest-type sample galaxies ($T < 2$) we find very small colour gradients at these z distances. It is, in fact, expected that the intrinsic colour gradients at these heights above the planes are smaller than those in the planes, where the young population contributes to the luminosity. At these z heights we are looking at the old-disk population, which is very uniform in colour, as was argued in Sect. 1.2.1.

The results presented in this section are consistent with those published previously (e.g., Elmegreen & Elmegreen,

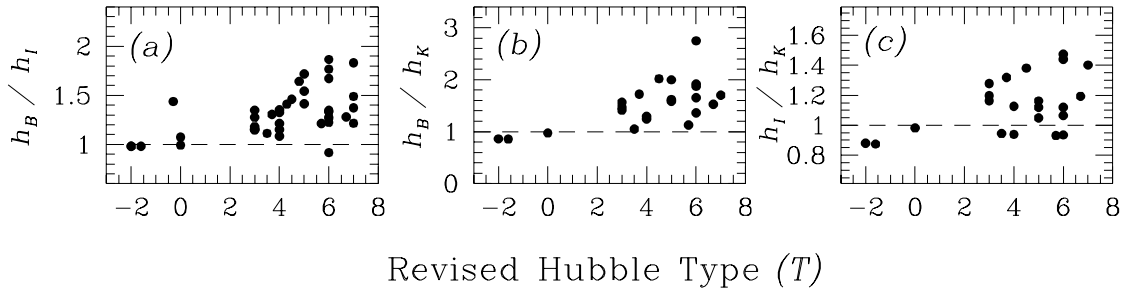

Fig. 5. Scale length ratios as a function of revised Hubble type derived from the profiles extracted parallel to the galaxies' major axes. The dashed lines indicate the locus of galaxies which do not show any scale length difference between passbands.

Table 4. Scale length ratios of the sample galaxies
Columns: (1) Scale length ratio; (2) (Sub)sample used; (4) Number of galaxies in the (sub)sample; (5) Resulting scale length ratio and standard deviation.

Gradient	Galaxy types	Number of Galaxies	Mean Ratio
(1)	(2)	(3)	(4)
h_B/h_I	$T > 2$	40	1.36 ± 0.22
	All types	45	1.32 ± 0.24
h_B/h_K	$T > 2$	22	1.65 ± 0.41
	All types	25	1.56 ± 0.46
h_I/h_K	$T > 2$	22	1.19 ± 0.17
	All types	25	1.15 ± 0.19

1984; Peletier et al., 1994, 1995a; de Jong, 1996a; and others), as will be shown in Sect. 4.3.

3.3 Correlations between gross galaxy properties

Since the sample we are dealing with is a diameter-selected sample of edge-on disk galaxies, a correction has to be applied to the observed parameters to represent a volume-limited sample (e.g., Davies, 1990). Because the sample galaxies were selected to have a minimum blue major axis diameter at 25 B-mag arcsec^{-2} (D^B_{25}) of 2.′2, we have created a selection bias against low surface brightness galaxies and galaxies with small scale lengths. The main implications of such a selection bias have been discussed by de Jong (1996b). In Fig. 6 we show the implications of our selection bias with respect to the disk properties of the observed sample galaxies in the (h_R, μ_0) plane.

The dashed and dotted lines in this figure represent the selection limits for a limiting diameter of 2.′2, using the 25 and 26 B-mag arcsec^{-2} isophotes, for comparison. The diameter-selection criterion used implies that our sample should only contain galaxies to the right of the selection limit in Fig. 6.

Although our sample selection was based on the $D_{\rm orig}$ diameter tabulated in the ESO-LV catalogue, this diameter was not determined at exactly the 25 B-mag arcsec^{-2} isophote (ESO-LV; Lauberts & Valentijn, 1989), but varies with galaxy type. For spiral galaxies the diameters correspond to approximately 26 B-mag arcsec^{-2} isophotes; for earlier types the corresponding isophotes are in the range from 25.0–25.6 B-mag arcsec^{-2}.

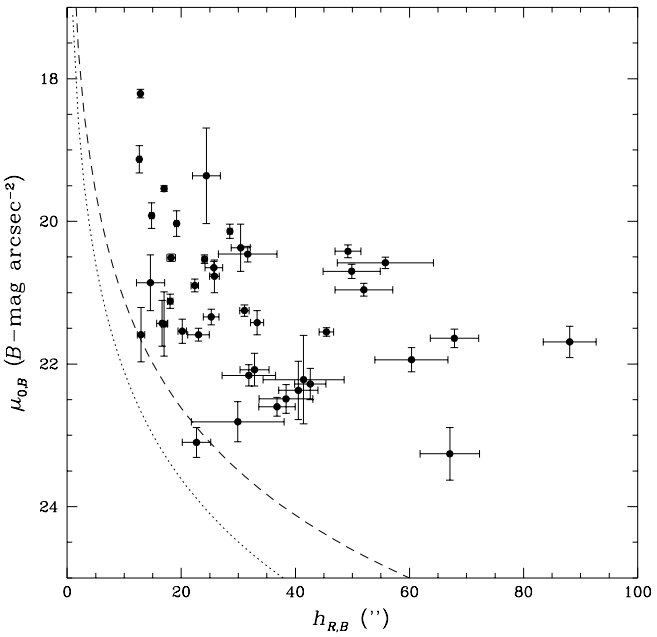

Fig. 6. Illustration of the effects of sample selection based on a diameter limit. The dashed line represents a diameter-selection limit (of 2.′2) at 25 B-mag arcsec^{-2}; the dotted line is the limit for a diameter-selection limit at 26 B-mag arcsec^{-2}.

As de Jong (1996b) remarks, since the number of galaxies in the sample will decrease as h_R^3 if all galaxies have the same scale length, it is not surprising that our sample does not contain galaxies with central B-band surface brightnesses fainter than about 23 B-mag arcsec^{-2}. Of course, the absolute lower limit for any galaxy to be included in the sample is $\mu_{0,B} = 25$ mag arcsec^{-2}.

3.3.1 Type dependences

In Fig. 7 we show the distributions of global K-band galaxy parameters as a function of Hubble type. We did not apply an inclination correction to the galaxy parameters, but since

we are dealing with edge-on galaxies, inclination *differences* do not play a significant role.

The distribution of (edge-on) K-band disk central surface brightnesses is rather flat (Fig. 7*a*), although with a large scatter. However, the latest-type sample galaxies ($T \geq 6$) show an indication that their disk central surface brightnesses may be fainter than those of the earlier types. Most likely, this effect is not the result of dust extinction, since the latest-type galaxies are not likely to contain more dust than the earlier and intermediate types, as was argued in Sect. 3.2. These results are consistent with those of de Jong (1996b).

Fig. 7*b* shows the distribution of the radial scale lengths of the galaxy disks, in kpc; we do not notice any clear correlation with galaxy type, apart from the observation that the earliest-type sample galaxies apparently have the smallest scale lengths, with only a small range of possible scale lengths compared to the range in the scale length distribution for galaxies of type $T > 2$. De Jong (1996b) noticed a possible lack of late-type galaxies with small scale lengths for his sample of 86 face-on disk galaxies, but remarked that this could be a selection effect. In fact, small galaxies (i.e., galaxies with small scale lengths) will have a greater possibility to be selected in a sample of edge-on galaxies than in a face-on galaxy sample, due to the line-of-sight integration through the galaxy disks. Therefore, his explanation seems to be valid, since we do not detect any lack of late-type disk galaxies with small scale lengths in our sample.

Finally, Fig. 7*c* shows the distribution of absolute I- and K-band magnitudes with Hubble type. Since in edge-on disk galaxies the luminosity is, at least for the later-type galaxies ($T > 2$), dominated by the disk luminosity, and thus the relation between the disk and the total absolute magnitude is approximately linear, we could have deduced the distribution of absolute magnitudes from Figs. 7*a* and *b* (de Jong, 1996b):

$$M_{\rm abs} \approx M_{\rm disk} \propto \mu_0 - 2.5 \log(2\pi h_R^2), \qquad (4)$$

where μ_0 is the (edge-on) disk central surface brightness, and $M_{\rm abs}$ and $M_{\rm disk}$ are the absolute magnitudes of the total galaxy and the disk component only, respectively.

Because the scale length distribution of Fig. 7*b* does not show any dependence on type, the distribution of absolute magnitudes reflects the distribution of central surface brightnesses with type, again consistent with de Jong (1996b).

3.3.2 Dust

The distribution of galaxy colours as a function of Hubble type is shown in Figs. 8*a–c* for the *(B–I), (B–K),* and *(I–K)* colours, respectively. We show the central disk colours, derived from the extrapolated central surface brightnesses, the colours of the total galaxy and those of the disk, denoted by different symbols. It is clear, that these colours follow the same distributions, although the scatter is large. In particular for the *(B–K)* and *(I–K)* colour distributions the colours derived from the total apparent magnitudes are systematically redder than the other two colour distributions. This is caused by dust, because the disk apparent magnitudes and the central surface brightnesses were obtained from ellipse fits to the outer disk regions, where the amount of dust is significantly lower than in the central plane. De Jong (1996b) notices a clear correlation between the colours of his 86 face-on spiral galaxies and galaxy type (but with a large scatter), whereas we do not find any such correlation. However, since our sample galaxies are heavily contaminated by dust, such a correlation, if intrinsic to the galaxies, may well be hidden by the interstellar dust.

In Figs. 8*d–f* we present colour-colour diagrams for our sample galaxies, again for the colours described above. Although the distributions follow each other closely and the correlations are generally tight, the correlation between total galaxy colours is systematically offset, again due to dust. This evidence is supported by the very red B–K colours of most of our galaxies, which are redder than those of bright giant ellipticals (with $B - K \sim 4.3$ [Peletier et al., 1994, 1995a]).

Therefore, Fig. 8 is completely dominated by dust effects; intrinsic colour gradients in the disks of galaxies, due to either metallicity or age gradients are too small to be observable, see also Sect. 4.3.

4 Discussion

4.1 Main observational results

From the statistical analysis of the global structure parameters of our sample of edge-on disk galaxies in the B, I, and K bands, in this Chapter we present the following main observational results:

- We found a correlation between the h_R/z_0 ratio and the revised Hubble type (Fig. 3*a*), in the sense that galaxies become systematically thinner when going from S0's to Sc's, whereas the later types (later than Sc) seem to be at least as thin as the Sc's.
- On average the colour gradients indicated by the scale length ratios increase from type Sa to at least type Scd. For galaxy types later than Scd, the colour gradients seem to become smaller again.
- The distribution of (edge-on) K-band disk central surface brightnesses is rather flat, although with a large scatter. However, the latest-type sample galaxies ($T > 6$) show an indication that their disk central surface brightnesses may be fainter than those of the earlier types. Most likely, this effect is not the result of dust extinction.
- We do not find a clear correlation between galaxy type and integrated, disk, or central colours. The scatter in the distributions is probably caused by dust.

4.2 Kinematic constraints from structure analysis

As was discussed in Sect. 1.1, once the h_R/z_0 ratio is known, one may be able to determine the maximum rotation of a disk from measurements of the vertical disk dispersion, although the theoretical predictions are based on assumptions that show large intrinsic scatter themselves. Van der Kruit & Searle (1982a) found a mean scale parameter ratio of $h_R/z_0 = 5.0 \pm 1.8$ for their sample of 8 edge-on disk galaxies (predominantly later-type spirals) in the optical J band, whereas de Grijs & van der Kruit (1996, Chapter 4) reported a mean ratio of $h_R/z_0 = 5.9 \pm 0.4$ based on the I-band characteristic length scales in their sample of 7 edge-on disk galaxies. These ratios are larger than the mean ratio found in this Chapter ($\langle h_R/z_0 \rangle = 3.7 \pm 1.3$).

To fit the observations of the maximum rotational velocity of disk-dominated Sc galaxies, h_R/z_0 needs to be of order 10 (Bottema, 1993). The discrepancy between the observational results and the theoretical prediction leads Bottema (1993) to the conclusion that, for realistic h_R/z_0 ratios, the stellar

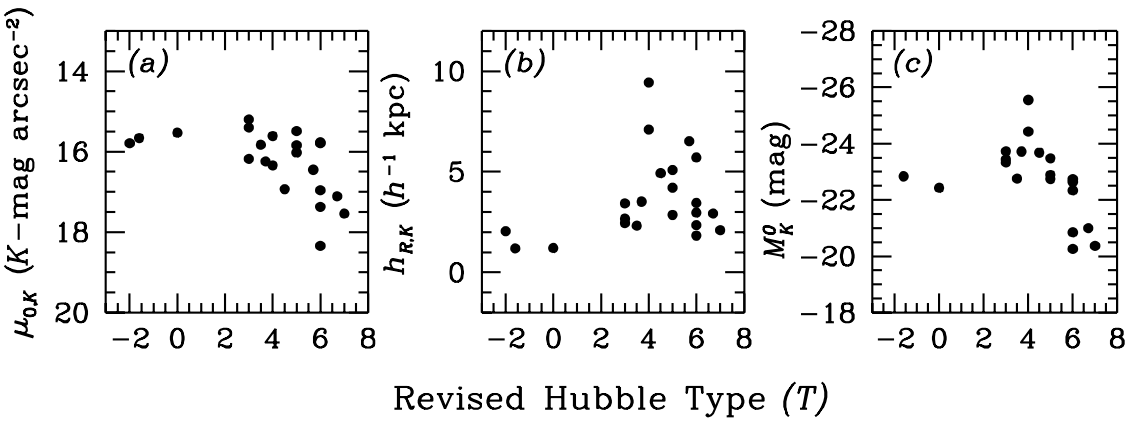

Fig. 7. Distribution of global K-band galaxy properties as a function of galaxy type: *(a)* Central disk surface brightnesses; *(b)* Disk radial scale lengths (in h^{-1} kpc); *(c)* Absolute magnitudes of the sample galaxies.

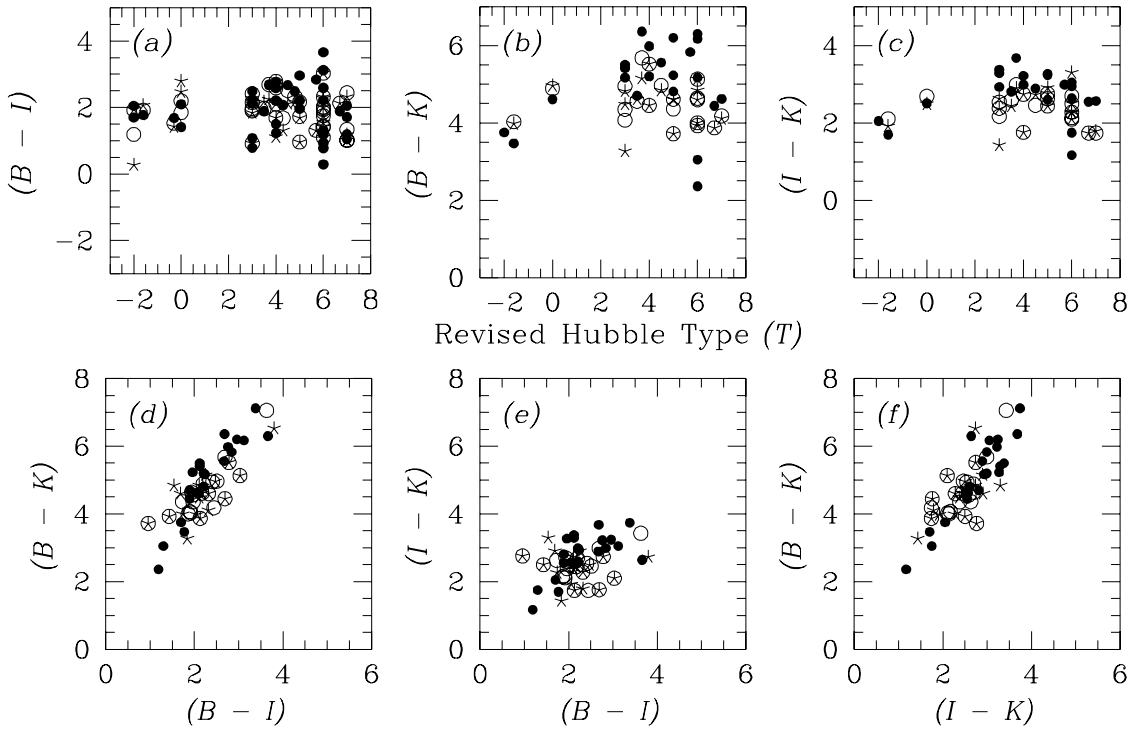

Fig. 8. Colour distributions of the sample galaxies: *(a)–(c)* Galaxy colours as a function of revised Hubble type; *(d)–(f)* Colour-colour diagrams. The filled dots denote central galaxy colours (based on the extrapolated central surface brightnesses), the open circles represent the galaxies' total colours, and the stars show the colours of the disks.

velocity dispersions only allow the disk to have a (theoretical) maximum rotation of on average $(63 \pm 10)\%$ of the observed maximum rotation. This is significantly less than implied by results of the so-called maximum disk fits (e.g., van Albada & Sancisi, 1986) that are widely used to model galaxy rotation curves, which predict a maximum-disk rotation of 85-90% of the observed rotation (Bottema, 1993).

Recent estimates of the scale parameters of our Galaxy (e.g., Kent et al., 1991; see Sackett, 1997, for an overview), yield a scale parameter ratio of $(h_R/z_0)_{\rm Gal} = 5.3 \pm 0.5$, which is consistent with the ratios published previously as well as with the data for external galaxies presented in this Chapter. However, although this ratio for our Galaxy is significantly less than the value of order 10 required theoretically (Bottema, 1993), Sackett (1997) argues that new structural and kinematical constraints are consistent with a Galactic maximum disk with reasonable mass-to-light ratio, of $2 \leq M/L_V \leq 7$.

In Sect. 3.1 we showed that the h_R/z_0 ratio of our sample galaxies correlates with revised Hubble type. This effect is not likely to be caused by the presence of a thick disk in

our earlier-type sample galaxies, since we used the thin disk scale parameters to derive the correlation (see also de Grijs & Peletier, 1997 [Chapter 7]). Part of the effect may be due to the distribution of the scale lengths among our sample galaxies, in the sense that the earlier-type galaxies tend to have smaller scale lengths. Moreover, van der Kruit & Searle (1982a) argue that the scale height is linearly dependent on the fraction of stellar to gas mass. Under this assumption, it is expected that the vertical scale parameter in the later-type galaxies is smaller than that for the earlier types. However, we cannot confirm this assumption on the basis of our observations.

4.3 Radial colour gradients and extinction

In this Chapter we show that the mean scale length ratios for the later-type ($T > 2$) disk galaxies in our sample range from $h_I/h_K = 1.15 \pm 0.19$ to $h_B/h_K = 1.65 \pm 0.41$, indicating large colour gradients in the disks. When comparing our results to those published previously we have to keep in mind the nature of our sample: since it consists solely of edge-on disk galaxies, the observed scale length ratios can be expected to be larger than similar ratios obtained from samples including less highly-inclined galaxies.

Most previously published scale length ratios favour large colour gradients in galaxy disks:

- For a large sample of face-on galaxies, Elmegreen & Elmegreen (1984) found a mean ratio of $h_B/h_I = 1.16 \pm 0.47$. Using Evans' (1994) models this corresponds to an average ratio of B to K-band scale length of about 1.32.
- Peletier et al. (1994, 1995a) present the results of a study of 37 Sb and Sc galaxies (uniform in orientation on the sky), for which they show that the B to K-band scale length ratio varies between 1.2 and 2, with a mean ratio of $h_B/h_K = 1.49 \pm 0.29$, comparable to our results.
- From de Jong's (1996a) scale length determinations of 86 face-on spiral galaxies, we find an average B to K-band scale length ratio $h_B/h_K = 1.22 \pm 0.23$
- From a study of the prototypical dusty galaxy NGC 253, Forbes & DePoy (1992) find $h_B/h_H = 1.25 \pm 0.05$.

Large colour gradients in galaxy disks between B and I band have also been reported by Kent (1986). However, from a sample of 33 disk galaxies, van der Kruit (1991) reported a small scale length ratio between the photographic J and F bands, $h_J/h_F = 1.07 \pm 0.13$.

The main problem when comparing scale lengths and scale length ratios determined by different authors is the radial fitting range used to derive the scale lengths (Sect. 2.1). However, if scale length ratios are calculated from scale lengths determined over the same radial fitting range in each passband, the differences between different determinations should be $\sim 10\%$ at maximum (Peletier et al., 1994).

Peletier et al. (1994, 1995a,b) argue that scale length ratios due to stellar population changes are of order 1.1–1.2 in the blue – near-infrared range. Two lines of evidence were used to arrive at this result: first, from observations of $T < 1$ type galaxies without much visible dust by Balcells & Peletier (1994), it was found that $h_B/h_I = 1.04 \pm 0.05$, corresponding to B to K-band scale length ratios of at most $h_B/h_K = 1.08 \pm 0.10$, using stellar population models of, e.g., Arimoto & Yoshii (1986). From metallicity gradients from HII regions in galaxy disks, Peletier et al. (1994, 1995a) argue that h_B/h_K is likely of order 1.17, using a simple single-age stellar population model. In the I vs. K range this contribution is likely to be less. Our observations of the scale length ratios in our earliest-type sample galaxies ($T < 1$) support this evidence (Fig. 5).

Therefore, the observed scale length ratios largely represent the galaxies' dust content.

Although the scale length ratios indicate an increasing dust content for galaxy types later than about $T = 3$ (Sb), the data suggests that the distribution of scale length ratios flattens or even decreases towards later types, as was also found from optical depth measurements (e.g., de Grijs et al., 1997 [Chapter 8]). This result is in accordance with the distribution found by Peletier & Balcells (1996).

5 Summary and Conclusions

The main conclusions we can draw from the analysis presented in this Chapter are:

- We found a correlation (although with a large scatter) between the h_R/z_0 ratio and galaxy type, in the sense that galaxies become systematically thinner when going from S0's to Sc's, whereas the later types (Sd's) seem to be at least as thin as the Sc's, but likely thicker.
- The average values found for the h_R/z_0 ratio are significantly smaller than the theoretical prediction of about 10 needed for maximum-disk rotation.
- On average the colour gradients indicated by the scale length ratios increase from type Sa to at least type Scd. For galaxy types later than Scd, the colour gradients seem to become smaller again.
- The observed scale length ratios (and thus the radial colour gradients) largely represent the galaxies' dust content.
- The distribution of (edge-on) K-band disk central surface brightnesses is rather flat, although with a large scatter. However, the latest-type sample galaxies ($T > 6$) show an indication that their disk central surface brightnesses may be fainter than those of the earlier types. Most likely, this effect is not the result of dust extinction.
- We do not find a clear correlation between galaxy type and integrated, disk, or central colours. The scatter in the distributions is probably caused by dust.

References

Aoki, T.E., Hiromoto, N., Takami, H., Okamura, S., 1991, PASJ 43, 755

Arimoto, N., Yoshii, Y., 1986, A&A 107, 135

Balcells, M., Peletier, R.F., 1994, AJ 107, 135

Barnaby, D., Thronson Jr., H.A., 1992, AJ 103, 41

Bottema, R., 1993, A&A 275, 16

Burstein, D., Heiles, C., 1978, ApJ 225, 40

Burstein, D., Heiles, C., 1984, ApJS 54, 33

Byun, Y.I., Freeman, K.C., Kylafis, N.D., 1994, ApJ 432, 114

Carlberg, R.G., 1987, ApJ 322, 59

Davies, J.I., 1990, MNRAS 244, 8

de Grijs, R., Peletier, R.F., 1997, A&A 320, L21 **(Chapter 7)**

de Grijs, R., Peletier, R.F., van der Kruit, P.C., 1997, A&A, in press **(Chapter 8)**

de Grijs, R., van der Kruit, P.C., 1996, A&AS 117, 19 **(Chapter 4)**
de Jong, R.S., 1996a, A&AS 118, 557
de Jong, R.S., 1996b, A&A 313, 45
de Jong, R.S., 1996c, A&A 313, 377
de Vaucouleurs, G., de Vaucouleurs, A., Corwin, H.G., Jr., Buta, R.J., Paturel, G., Fouqué, P., 1991, Third Reference Catalogue of Bright Galaxies, Springer-Verlag: New York **(RC3)**
Disney, M.J., Davies, J.I., Phillipps, S., 1989, MNRAS 239, 939
Elmegreen, D.M., Elmegreen, B.G., 1984, ApJS 54,127
Evans, R., 1994, MNRAS 266, 511
Fall, S.M., 1983, in: Internal Kinematics and Dynamics of Galaxies, IAU Symposium 100, ed. Athanassoula, E., Dordrecht: Reidel, p. 391
Fall, S.M., Efstathiou, G., 1980, MNRAS 193, 189
Forbes, D.A., DePoy, D.L., 1992, A&A 259, 97
Freeman, K.C., 1970. ApJ 160, 811
Giovanelli, R., Haynes, M.P., Salzer, J.J., Wegner, G., Da Costa, L.N., Freudling, W., 1994, AJ 107, 2036
Hamabe, M., Kodaira, K., Okamura, S., Takase, B., 1979, PASJ 31, 431
Hamabe, M., Kodaira, K., Okamura, S., Takase, B., 1980, PASJ 32, 197
Hamabe, M., Wakamatsu, K., 1989, ApJ 339, 783
Huizinga, J.E., 1994, Ph.D. Thesis, Groningen University
Jensen, E.B., Thuan, T.X., 1982, ApJS 50, 421
Kent, S.M., 1986, AJ 91, 1301
Kent, S.M., Dame, T.M., Fazio, G., 1991, ApJ 378, 131
Knapen, J.H., van der Kruit, P.C., 1991, A&A 248, 57
Kuchinski, L.E., Terndrup, D.M., 1996, AJ 111, 1073
Kylafis, N.D., Bahcall, J.N., 1987, ApJ 317, 637
Larson, R.B., Tinsley, B.M., 1978, ApJ 219, 46
Lauberts A., Valentijn, E.A., 1989, The Surface Photometry Catalogue of the ESO-Uppsala Galaxies, ESO **(ESO-LV)**
Mathewson, D.S., Ford, V.L., Buchhorn, M., 1992, ApJS 81, 413
Peletier, R.F., 1993, A&A 271, 51
Peletier, R.F., Balcells, M., 1996, in: Spiral Galaxies in the Near-IR, eds. Minnitti, D., Rix, H.-W., ESO/MPA Workshop, p. 48
Peletier, R.F., Balcells, M., 1997, New Astr. 1, 349
Peletier, R.F., Valentijn, E.A., Moorwood, A.F.M., Freudling, W., 1994, A&AS 108, 621
Peletier, R.F., Valentijn, E.A., Moorwood, A.F.M., Freudling, W., 1995a, in: The Opacity of Spiral Disks, ed. Davies, J., NATO Advanced Research Workshop, p. 243
Peletier, R.F., Valentijn, E.A., Moorwood, A.F.M., Freudling, W., Knapen, J.H., Beckman, J.E., 1995b, A&A 300, L1
Peletier, R.F., Willner, S.P., 1992, AJ 103, 1761
Richter, O.-G., Tammann, G.A., Huchtmeier, W.K., 1987, A&A 171, 33
Rieke, G.H., Lebofsky, M.J., 1985, ApJ 288, 618
Sackett, P.D., 1997, ApJ 483, 103
Sandage, A., 1986, A&A 161, 89
Sasaki, T., 1987, PASJ 39, 849
Schmidt, K.-H., Boller, T., 1992, Astron. Nachr. 313, 189
Searle, L., Sargent, W.L.W., Bagnuolo, W.G., 1973, ApJ 179, 427
Shaw, M.A., Gilmore, G., 1990, MNRAS 242, 59
Terndrup, D.M., Davies, R.L., Frogel, J.A., DePoy, D.L., Wells, L.A., 1994, ApJ 432, 518
Tinsley, B.M., Larson, R.B., 1978, ApJ 221, 554
Toomre, A., 1964, ApJ 139, 1217
van Albada, T.S., Sancisi, R., 1986, Philos. Trans. R. Soc. London, Ser. A 320, 447
van der Kruit, P.C., 1987, A&A 173, 59
van der Kruit, P.C., 1991, in: The World of Galaxies, eds. Corwin, H.G., Bottinelli, L., New York: Springer, p. 256
van der Kruit, P.C., Searle, L., 1981a, A&A 95, 105
van der Kruit, P.C., Searle, L., 1981b, A&A 95, 116
van der Kruit, P.C., Searle, L., 1982a, A&A 110, 61
van der Kruit, P.C., Searle, L., 1982b, A&A 110, 79
Wainscoat, R.J., Hyland, A.R., Freeman, K.C., 1990, ApJ 348, 85